Oscillatory Neck Instability of Spatial Bright Solitons in Hyperbolic Systems

S.-P. Gorza, P. Kockaert, Ph. Emplit, and M. Haelterman

Service OPERA-photonique, Université libre de Bruxelles (ULB), 50 Avenue F. D. Roosevelt, CP194/5 B-1050 Bruxelles, Belgium

(Received 15 October 2008; published 2 April 2009)

The breakup of spatial bright optical solitons due to oscillatory neck instability is experimentally studied by propagating a laser beam in normally dispersive and self-focusing Kerr media. This intriguing and unusual phenomenon, recently predicted for solitons of the (2 + 1)-dimensional hyperbolic nonlinear Schrödinger (NLS) equation, is observed in the spatially resolved temporal spectrum. The snake instability that is known to occur in hyperbolic systems is also demonstrated to validate our experimental approach. Our results not only apply to photonics but also to other fields of physics, such as hydrodynamics or plasma physics, in which the hyperbolic NLS equation is used as a canonical model.

DOI: 10.1103/PhysRevLett.102.134101 PACS numbers: 05.45.Yv, 42.65.Sf, 42.65.Tg, 42.65.Wi

Symmetry-breaking instability is one of the most remarkable physical phenomena that occurs in nonlinear media. Among these phenomena, the symmetry-breaking instability of plane solitary waves has attracted particular attention and was first formulated for soliton solutions of the nonlinear Schrödinger (NLS) equation and the Korteweg–de Vries equation [1–3]. In modern science, the NLS equation plays a major role by providing a canonical description of the dynamics of quasimonochromatic waves in weakly nonlinear media and therefore is naturally encountered in a variety of fields such as plasma physics, hydrodynamics, optics or in the description of Bose-Einstein condensates [3,4]. In a seminal work, Zakharov and Rubenchik [1] demonstrated that the soliton solution of the (1 + 1)-dimensional NLS equation is always modulationally unstable against perturbations involving higher dimensions. More specifically, they showed, in the context of optics, that bright spatial soliton beams spontaneously breakup when propagating in dispersive media. Moreover, they predicted that the instability scenario strongly differs between positive (hyperbolic NLS equation) and negative (elliptic NLS equation) dispersion. On the one hand, in anomalous dispersive media ruled by the elliptic NLS equation, bright spatial solitons undergo a *neck* type instability that causes spatiotemporal oscillations of their amplitude. Several experiments in optics report on the observation of this neck instability [5–7]. On the other hand, in normally dispersive media ruled by the hyperbolic NLS equation, solitons exhibit a *snake* type instability characterized by a periodic undulation of the soliton beam axis. Experimental demonstrations of the snake instability were reported in hydrodynamics [8] and in optics [9,10]. In these latter works, the transverse snake instability of a spatially extended temporal bright soliton was observed. In normally dispersive bulk media, Y-shaped unstable modes are responsible for axial and conical emission [11].

In early theoretical works on the (2 + 1)-dimensional hyperbolic NLS equation, the snake type instability is presented as being the only instability mechanism for the bright solitons [1,3,4]. However, recently, the existence of a novel mechanism that can be interpreted as an ''oscillating'' neck instability has been identified [12,13].

In this Letter, we propose an experimental study of this new fundamental instability mechanism. More precisely, temporal instabilities of spatial bright solitons of the two-dimensional hyperbolic NLS equation are experimentally studied by propagating a laser beam in a self-focusing and normally dispersive nonlinear planar waveguide. We first show that these solitons are unstable against spatiotemporal periodic modulation of their amplitude, confirming in this way the new ''oscillating'' neck instability mechanism. We also demonstrate that the bright spatial soliton beams undergo a snake type instability as theoretically predicted in the early theoretical works. These results are relevant to many research fields as far as the two-dimensional hyperbolic NLS equation is used as a model. It is encountered for instance to describe deep-water gravitational waves [14] or cyclotron waves in plasma [15]. In optics, this equation provides a standard description for the propagation of optical beams in normally dispersive planar waveguides with positive Kerr effect [16]. In dimensionless variables, this equation is

$$i\frac{\partial \psi}{\partial z} + \frac{1}{2}\frac{\partial^2 \psi}{\partial x^2} - \frac{1}{2}\frac{\partial^2 \psi}{\partial t^2} + |\psi|^2\psi = 0, \qquad (1)$$

where x is the transverse (in-plane) coordinate, z is the propagation coordinate, and t is the time. These variables are normalized with respect to the beam width x_0, the diffraction length $L_D = kx_0^2$, and the time $t_0 = (k'' L_D)^{1/2}$, respectively, where k is the guided-mode propagation constant and $k'' = \partial^2 k/\partial\omega^2 > 0$ the group velocity dispersion coefficient. The amplitude ψ is linked to the slowly varying envelope of the electromagnetic field E by $\psi = (\gamma L_D)^{1/2} E$, where $\gamma = 2\pi n_2/(\lambda L_{\text{eff}})$, λ is the wavelength, n_2 is the positive Kerr coefficient, and L_{eff} is the effective core thickness of the waveguide.

The bright spatial soliton solution of Eq. (1) is $\psi = \mathrm{sech}(x)\exp(iz/2)$. However, because of chromatic dispersion [the third term in Eq. (1)], spatial solitons are unstable against periodic temporal perturbations of the form $\epsilon(x, z, t) = \epsilon_0(u_1 + iu_2)e^{iz/2}$ with $u_{1,2} = [\phi_{1,2}(x)e^{i\Omega t+\Gamma z} + \text{c.c.}]$, where the eigenmodes $\phi_{1,2}(x)$ are complex functions of the transverse coordinate x, Ω is the temporal modulation frequency, and the instability gain is given by the real part of Γ. Results reported in Ref. [1] and subsequent analytical or numerical studies (see, e.g., Ref. [12] and references therein) show that the eigenmode is an antisymmetric function, which reveals the onset of a zigzag-shaped deformation of the soliton. This is illustrated in Fig. 1 (left column) by numerical simulation of the propagation of a spatial soliton seeded by an antisymmetric perturbation (odd ϕ function). However, in Refs. [12,13], the existence of a new branch in the instability gain spectrum has been demonstrated. This branch is associated with symmetric eigenmodes and complex Γ values, and therefore corresponds to an oscillatory neck instability. This result is rather surprising in the sense that the spatiotemporal self-focusing associated with the neck instability is totally counterintuitive in the normal dispersion regime. Our numerical simulations with symmetric seeds confirm this unexpected result, as shown in Fig. 1 (right hand side). Note that snake and neck type instabilities also coexist in the case of normal group velocity dispersion for solitons in quadratic-media (self-trapping due to wave-mixing processes) [17] and for the radially symmetric ground state solution of the NLS equation with two transverse dimensions [18].

Experiments were performed with a 12 mm planar waveguide made up of a 1.6 μm-thick guiding layer of $Al_{0.18}Ga_{0.82}As$ on the top of a 4 μm-thick cladding of $Al_{0.24}Ga_{0.76}As$. The laser source is a picosecond mode-locked fiber laser (10 MHz repetition rate, 5 ps full-width at half maximum [FWHM]) amplified by an erbium/ytterbium-doped fiber amplifier. The laser beam at the fiber laser output is first collected by a $\times 16$ microscope objective and then passes successively through a quarter-wave plate, a half-wave plate, and a free-space isolator. The isolator is used to avoid any back-reflection into the amplifier and sets the beam polarization horizontally to excite the TE_0 mode of the waveguide. The laser beam is then coupled into the waveguide with a 16.5 μm width (FWHM). Our 12 mm-long waveguide is therefore $9.2L_D$ long. At the waveguide output, the beam, collected by a $\times 60$ microscope objective, is directed to an optical spectrum analyzer and a two-dimensional spectrometer to image the spatially resolved spectrum on an infrared vidicon camera. The wavelength has been set to 1.535 μm, slightly below the semiconductor half band-gap to ensure a positive Kerr nonlinearity ($n_2 = 1.6 \times 10^{-17}$ m^2/W) together with normal dispersion ($k'' = 1.04 \times 10^{-24}$ s^2/m) and low nonlinear absorption [19,20].

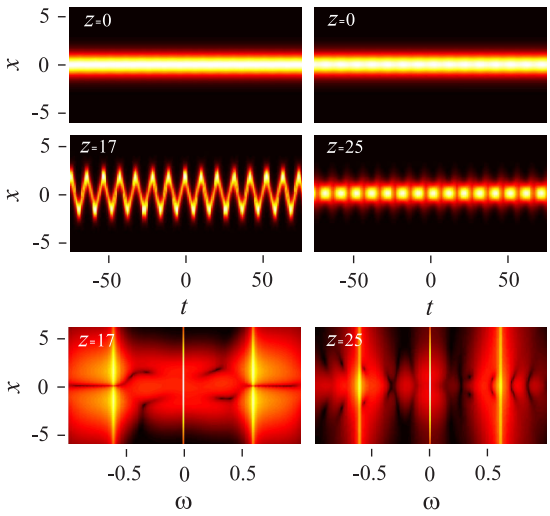

FIG. 1 (color online). Numerical simulation of the breakup of a spatial soliton in hyperbolic systems. Left (right) column: snake (neck) type instability. Bottom: density plots of the spatially resolved temporal spectrum (logarithmic scale).

The spatiotemporal profile of the beam, as depicted in Fig. 1, can not be easily recorded because of the time scale involved in the instability process, the period of the temporal modulation being typically around 300 fs. However, because the formation of spatiotemporal periodic structures leads to the appearance of sidebands in the temporal spectrum, the soliton instability can be easily studied in the frequency domain. Moreover, through the use of a camera, the spectrum at all values of the transverse coordinate x can be recorded at once, providing the "spatially resolved" spectrum. As shown at the bottom of Fig. 1, the neck instability being associated with symmetric eigenmodes, the spatial profile of its frequency sidebands is symmetric. Conversely, being characterized by odd eigenmodes, the snake instability spectrum has frequency sidebands with antisymmetric spatial profiles. The sideband antisymmetry is revealed in Fig. 1 (bottom left) by the dark horizontal stripes located at the center of the soliton beam.

Figure 2 shows the spatially resolved spectrum at the output of the waveguide. At low power, the beam extends up to 190 μm FWHM due to diffraction. As can be seen, the profile along the frequency axis is slightly asymmetric and ribbed because of the self-phase modulation experienced in the amplifier. As the input power increases, the width of the output beam decreases, with the narrowest profile occurring at a power of 780 W as shown in Fig. 2. At the same time, a well developed spectral structure, with the outermost peaks being the most intense, appears, as expected from the theory of self-phase modulation induced spectral broadening [21]. The spatial width of these peaks are of 34 μm FWHM, which is larger than the input beam width because of losses, estimated to be around 3.8 dB/cm. Note that, because nonlinearity in the trailing and leading edges of the pulses is too low to compensate

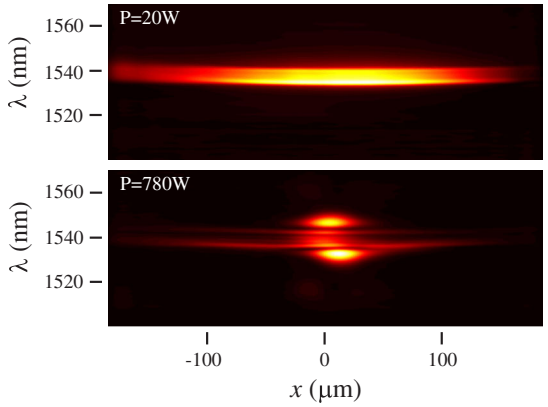

FIG. 2 (color online). Experimental results showing the formation of a spatial soliton at the output of a 12 mm-long planar waveguide. At high power, strong spatial confinement of the energy is observed and a spatial soliton is formed. Diffraction in the pulse wings manifests itself as bright stripes near the pulse spectrum center.

for diffraction, the spatially resolved spectrum exhibits low-amplitude broad spatial profiles near the central frequency.

The spectral sidebands are not visible in Fig. 2 because their amplitudes are too low in comparison with the main peaks. However, when plotted in logarithmic scale as in Fig. 3, the recorded spatially resolved spectral intensity $[|\tilde{S}(\lambda, x)|^2]$ reveals the spectral sidebands as well as their spatial profile. At the bottom of Fig. 3, the spatial intensity profiles of the main central peak located at 1530 nm and of the sideband at 1512 nm have been plotted together. Clearly, the spatial intensity profile of the sidebands have their maxima located at the beam center. In the temporal domain, the sidebands naturally lead to a periodic modulation of the soliton amplitude, i.e., a neck instability since both the soliton beam and the sidebands spatial profiles have the same symmetry. Note that the sideband profile is narrower than the soliton profile but has broader wings, which is in good agreement with numerical simulations (see inset in Fig. 3).

In Fig. 4, the input and output spectra at the beam center have been plotted when the soliton is formed. These spectra were acquired by means of an optical spectrum analyzer. We observe the existence of two symmetric low-amplitude sidebands in the input beam spectrum. These sidebands are generated in the amplifier by modulational instability that is unavoidable at the soliton power. Their spatial profile having the same shape as the soliton beam, these sidebands act as a natural seed for the neck instability. At the output, the spectrum (solid line) clearly shows the amplification of the sidebands and the generation of higher-order harmonics. We can therefore reasonably state that our observations constitute a genuine proof of the intriguing phenomenon of neck instability in the hyperbolic NLS equation, as recently predicted theoretically in Ref. [13].

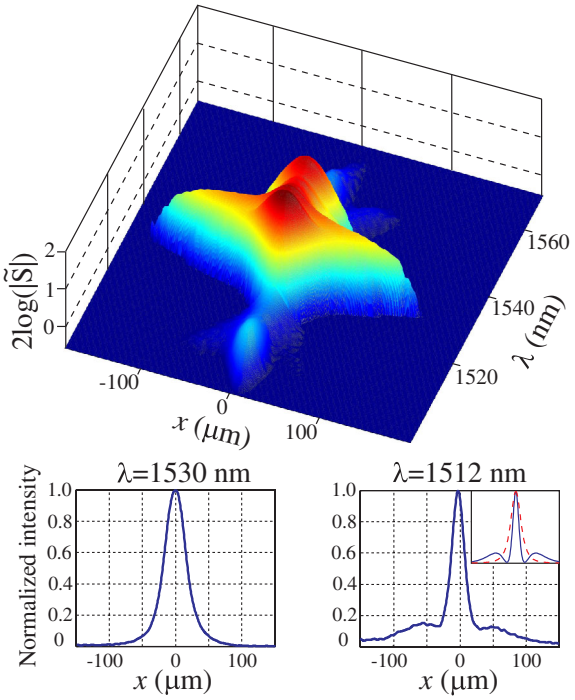

FIG. 3 (color online). Top: 3D-plot of the spatially resolved temporal spectrum of the soliton beam shown in Fig. 2. The logarithm of the spectral density ($|\tilde{S}|^2$) is plotted to reveal the spatial structure of both the soliton beam and the spectral sidebands. These sidebands are the signature of the neck type instability of the soliton beam. Bottom: spatial profiles at two different wavelengths, left: in the main spectral peak, right: in the sideband. The inset shows the corresponding spatial profiles computed from numerical simulation of the soliton propagation.

As can be seen in Fig. 5 (see also Ref. [22]), asymmetric spatial sidebands have also been observed at the output of the waveguide at soliton power. The sidebands intensity profile now clearly shows a dip at the soliton center (as in

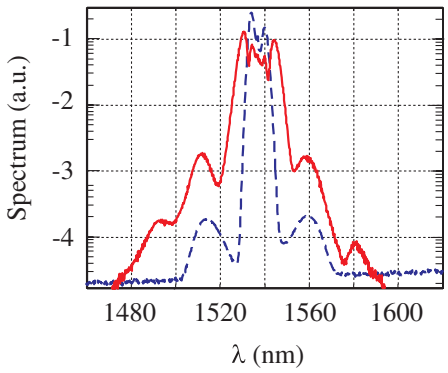

FIG. 4 (color online). Experimental input (dashed line) and output (solid line) normalized spectra measured at the beam center in the same conditions as in Fig. 3.

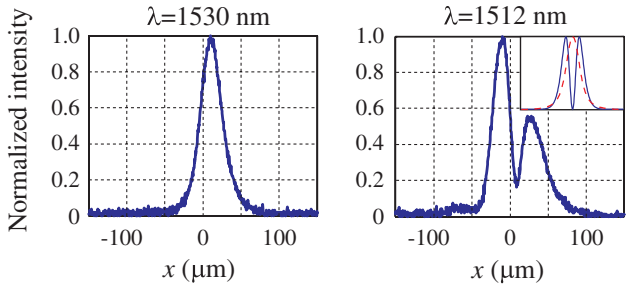

FIG. 5 (color online). Experimental signature of the snake instability of the bright soliton. See caption of Fig. 3 for explanation.

Fig. 1), a spectral feature that reveals the antisymmetric nature of the sideband profiles and leaves no doubt about the development of the snake instability. Note that we have obtained antisymmetric sidebands only when injecting the beam in the vicinity of small defects of the entrance face of the waveguide. Since the beam at the output of the waveguide never exhibits any significant distortions, we concluded that the defects only slightly affect the input beam phase profile, without preventing soliton formation. Through numerical simulations, we have observed that such small asymmetric phase distortions are sufficient to seed the snake instability. The asymmetry observed in the output spatial profile of the sidebands (see Fig. 5) can be easily explained by the fact that both the snake and the neck instabilities coexist in the system and that they are simultaneously seeded. Note, however, that the small asymmetry of the seed is compensated by the larger gain of the snake instability with respect to the neck instability (see Ref. [13]). The frequency sidebands being amplified by almost 10 dB, our experiment constitutes an experimental evidence of the snake instability of the bright soliton of the (2 + 1)D hyperbolic NLS equation. This observation has recently been the object of a detailed report [23]. We described it here briefly to show the validity of the experimental approach that we chose to identify the neck instability.

In summary, through the experimental study of the propagation of a spatial soliton in a normally dispersive and self-focussing planar semiconductor waveguide, we have provided the first experimental demonstration of the counterintuitive neck type modulational instability of the spatial bright soliton of the hyperbolic (2 + 1)D cubic nonlinear Schrödinger equation [12,13]. Our results confirm that space-time coupling leads to complex behaviors in nonlinear systems since in a (1 + 1)D system (e.g., an optical fiber), continuous waves are stable when propagating in a normally dispersive focusing Kerr medium [21]. The neck instability has been identified through the analysis of the spatially resolved spectra where the amplification of spectral sidebands with symmetric spatial profiles was clearly identified. Comparison with the asymmetric spatial profiles of the sidebands associated with the snake instability allowed us to validate our experimental approach.

The authors are grateful to R. Baets and D. Taillaert (INTEC, Ghent University) for providing the sample. This work was supported by the Belgian Science Policy Office under Grant No. IAP6-10 and by the Fonds de la Recherche Fondamentale Collective, Grant No. F 2.4513.06. S.-P. Gorza acknowledges the support of the Fonds de la Recherche Scientifique (F.R.S.-FNRS, Belgium).

[1] V. E. Zakharov and A. M. Rubenchik, Sov. Phys. JETP **38**, 494 (1974).
[2] B. B. Kadomtsev and V. I. Petviashvili, Sov. Phys. Dokl. **15**, 539 (1970).
[3] For recent review on instabilities, see Y. S. Kivshar and D. E. Pelinovsky, Phys. Rep. **331**, 117 (2000).
[4] K. Rypdal and J. J. Rasmussen, Phys. Scr. **40**, 192 (1989).
[5] A. V. Mamaev, M. Saffman, and A. A. Zozulia, Europhys. Lett. **35**, 25 (1996).
[6] X. Liu, K. Beckwitt, and F. Wise, Phys. Rev. Lett. **85**, 1871 (2000).
[7] S. D. Jenkins *et al.*, Phys. Rev. Lett. **95**, 203902 (2005).
[8] E. D. Brown *et al.*, J. Fluid Mech. **204**, 263 (1989).
[9] S. P. Gorza *et al.*, Phys. Rev. Lett. **92**, 084101 (2004).
[10] S. P. Gorza, Ph. Emplit, and M. Haelterman, Opt. Lett. **31**, 1280 (2006).
[11] M. A. Porras *et al.*, Phys. Rev. A **76**, 011803(R) (2007).
[12] D. E. Pelinovsky, Math. Comput. Simul. **55**, 585 (2001).
[13] B. Deconinck, D. E. Pelinovsky, and J. D. Carter, Proc. R. Soc. A **462**, 2039 (2006).
[14] V. E. Zakharov, J. Appl. Mech. Tech. Phys. **2**, 190 (1968).
[15] J. R. Myra and C. S. Liu, Phys. Fluids **23**, 2258 (1980).
[16] V. E. Zakharov and A. B. Shabat, Sov. Phys. JETP **34**, 62 (1972).
[17] A. V. Buryak *et al.*, Phys. Rep. **370**, 63 (2002).
[18] K. Germaschewski *et al.*, Physica (Amsterdam) **151D**, 175 (2001).
[19] J. S. Aitchison *et al.*, IEEE J. Quantum Electron. **33**, 341 (1997).
[20] S. Adachi, Phys. Rev. B **38**, 12345 (1988).
[21] G. P. Agrawal, *Nonlinear Fiber Optics* (Academic Press, San Diego, 2001).
[22] See EPAPS Document No. E-PRLTAO-102-068913 for the 3D-plot of the spatially resolved spectrum for the snake type instability. For more information on EPAPS, see http://www.aip.org/pubservs/epaps.html.
[23] S.-P. Gorza and M. Haelterman, Opt. Express **16**, 16935 (2008).